Structural Implications of Anomalous Thermal Expansion and Glass-Like Dielectric Response in Pyridinium Halogenoaurates

Marek Szafrański

Faculty of Physics, Adam Mickiewicz University, Umultowska 85, 61−614 Poznań, Poland

Received: July 7, 2005; In Final Form: September 14, 2005

The crystals of $[C_5NH_6]^+[AuCl_4]^-$, $[C_5NH_6]^+[AuBr_4]^-$, and $[C_5NH_6]^+[AuI_4]^-$ have been studied by single-crystal X-ray diffraction and dielectric spectroscopy. The structures of the chloride and bromide are isosymmetric, with the monoclinic space group *C*2/*m*, and both are built of sheets of pyridinium cations and tetrahalogenoaurate anions alternately arranged in the direction [001]. The anomalous thermal expansion and dielectric response characteristic of dipolar glass formation observed in these compounds have been interpreted in terms of the development of the short-range dipolar order and the competition between the ferroelectric and antiferroelectric interactions. The frustration of dipolar interactions, leading to glassy behavior, results from the strongly anisotropic properties of the layered crystal structure. These features have not been observed for $[C_5NH_6]^+[AuI_4]^-$, which crystallizes in the space group $P2_1/c$ and exhibits a nonlayered structural packing because of the larger size of the anion.

Introduction

The discovery of dipolar glassy states in $Rb_{1-x}(NH_4)_xH_2PO_4$ (RADP) solid solutions[1−3] has initiated considerable interest in the new class of materials known presently as dipolar glasses. These materials, a subgroup of orientational glasses, are commonly regarded as electric analogues of magnetic spin-glasses. In RADP crystals, the glass state originates from frustration effects due to the competing ferroelectric and antiferroelectric interactions. The dipolar relaxational dynamics in these compounds is related to the H-atom dynamics in the hydrogen bonds; hence, the alternative term for them is "proton glasses". The same mechanism is responsible for the glassy properties in mixed betaine crystals: antiferroelectric betaine phosphate, $(CH)_3NCH_2COO{\cdot}H_3PO_4$ (BP), and ferroelectric betaine phosphite, $(CH)_3NCH_2COO{\cdot}H_3PO_3$ (BPI). At intermediate concentrations of $(BP)_x(BPI)_{1-x}$, the long-range electric order is suppressed, and the dipolar moments freeze at low temperatures into random configurations, producing an orientational glass state.[4] A similar procedure of mixing two compounds with antiferroelectric and ferroelectric order was recently applied to obtain orientational glasses based on the pyridinium salts.[5] It has been shown that ferroelectric pyridinium tetrafluoroborate, $C_5H_6NBF_4$, and antiferroelectric pyridinium hexafluorophosphate, $C_5H_6NPF_6$, form solid solutions $C_5H_6N(BF_4)_{1-x}(PF_6)_x$ in the whole composition range and, in the range $0.3 < x < 0.7$, exhibit glassy properties at temperatures much higher than the archetypal proton glass RADP or $(BP)_x(BPI)_{1-x}$. In $C_5H_6N(BF_4)_{1-x}(PF_6)_x$ solutions, the dipolar relaxation dynamics originates from ionic motions, and the frustration effect leads to randomly distributed configurations of the pyridinium dipoles. Apparently, the strategy to produce glassy behavior in all of the above-mentioned systems relies on the mixing of two nearly isostructural crystals with competing long-range interactions. The substitutional disorder is also characteristic of other orientational glasses, such as a model $KBr_{1-x}(CN)_x$.[3] However, it is obvious that, even for very proximate crystals, their structures are not perfectly identical. Consequently, a structural nonhomogeneity is created on the microscopic level, leading to random local fields and to a distribution of activation energies of the relaxators. This also implies the nonzero Edwards−Anderson order parameter, even in the high-temperature phases.[6] Thus, the situation is more complex than that in classical spin-glasses, in which there is no structural contribution to their glassy behavior. Therefore, it still remains a challenging task to look for pure systems, which could exhibit a dipolar glass phenomenon. Such properties were reported recently for $TlNO_2$[7] and CuCN,[8] which do not transform to the completely ordered states upon normal cooling, but rather form orientational glasses. Potential candidates for such studies can also be pyridinium tetrahalogenoaurates of a general formula $PyAuX_4$, where Py $= [C_5NH_6]^+$ and X = Cl, Br, or I. The latter conclusion is suggested by the earlier results of NMR,[9] NQR,[10] and calorimetric and dielectric[11] studies. In this paper, we discuss the structure−property relationships in this group of pyridinium salts. Among the $PyAuX_4$ compounds, only the structure of $PyAuCl_4$ has previously been determined.[12] Therefore, we complemented the structural data with the structures of $PyAuBr_4$ and $PyAuI_4$. The structural information combined with the results of dilatometric and dielectric spectroscopy measurements has provided an explanation of dipolar glass formation in these compositionally homogeneous systems.

Experimental Section

The $PyAuX_4$ compounds were synthesized by dissolving stoichiometric amounts of PyX and AuX_3 in water. The substances obtained were purified by recrystallization from the acidified water solutions. Small, dark-brown $PyAuBr_4$ and $PyAuI_4$ crystals, and yellow, transparent $PyAuCl_4$ crystals were grown by slow evaporation at room temperature. For dielectric measurements, the crystalline material was ground into a fine powder and then pressed into pellets 0.5−1 mm thick and 13 mm in diameter. Gold electrodes were deposited on the large surfaces of the samples by evaporation in a vacuum. Measurements of complex electric permittivity were carried out in the frequency range of 1 kHz to 13 MHz using an HP 4192A

10.1021/jp053714a CCC: $30.25
Published on Web 10/18/2005

TABLE 1: Crystal Data and Refinement Details for $PyAuBr_4$ and $PyAuI_4$ at 295 K

chemical formula,	$[C_5NH_6]^+[AuBr_4]^-$	$[C_5NH_6]^+[AuI_4]^-$
formula weight	596.71	784.67
crystal size (mm^3)	0.3× 0.05 × 0.05	0.15× 0.10 × 0.06
crystal system, space group	monoclinic, *C*2/*m*	monoclinic, $P2_1/c$
unit-cell dimensions	$a = 11.226(3)$ Å, $b = 11.919(2)$ Å, $c = 4.158(5)$ Å, $\beta = 101.87(6)$ deg	$a = 8.732(6)$ Å, $b = 9.715(2)$ Å, $c = 7.861(2)$ Å, $\beta = 94.92(4)$ deg
Z, volume, density (calcd)	2, 544.5(7) $Å^3$, 3.640 Mg/m^3	2, 664.4(5) $Å^3$, 3.922 Mg/m^3
absorption coefficient	28.131 mm^{-1}	20.319 mm^{-1}
theta range for data collection	2.52−27.06 deg	3.14−25.05 deg
reflections collected/unique	1546/406 ($R_{int} = 0.0562$)	2427/1164 ($R_{int} = 0.0807$)
refinement method	full-matrix least-squares on F^2	full-matrix least-squares on F^2
data/restrains/parameters	406/0/30	1164/0/53
goodness-of-fit on F^2	1.048	0.944
final *R* indices [$I > 2\sigma(I)$]	R1 = 0.0400, wR2 = 0.0894	R1 = 0.0403, wR2 = 0.0977
all data	R1 = 0.0798, wR2 = 0.0984	R1 = 0.1182, wR2 = 0.12
max ΔF peak and hole ($e/Å^3$)	2.34, −0.779	2.693, −1.375
extinction coefficient	0.0029(8)	0.0101(10)

TABLE 2: Atomic Coordinates and Equivalent Isotropic Displacement Parameters for $PyAuBr_4$ and $PyAuI_4$

	x/*a*	*y*/*b*	*z*/*c*	U_{eq}[a]
		$PyAuBr_4$		
Au	0.5	0.5	0.5	0.041(1)
Br	0.3532(15)	0.3573(1)	0.5556(5)	0.063(1)
C(1)/N	0.104(2)	0.5	0.904(7)	0.082(9)
C(2)	0.057(2)	0.4025(14)	0.946(5)	0.069(8)
		$PyAuI_4$		
Au	0	0.5	0.5	0.047(1)
I(1)	−0.0002	0.8174(2)	0.7549(2)	0.081(1)
I(2)	0.3008(1)	0.4980(3)	0.5271(2)	0.073(1)
C(1)	0.491(11)	0.380(3)	0.032(4)	0.15(2)
C(2)	0.359(7)	0.449(8)	0.046(5)	0.16(3)
C(3)	0.390(8)	0.929(7)	0.519(5)	0.144(16)

[a] U_{eq} is defined as one-third of the trace of the orthogonalized U_{ij} tensor.

impedance analyzer. The amplitude of the ac-measuring electric field did not exceed 2 V/cm. The temperature of the sample was changed in the range of 80−300 K at a rate of 0.5 K/min.

The room-temperature X-ray diffraction data sets were collected on a KUMA-KM4 diffractometer equipped with graphite-monochromated Mo *K*α radiation. The $\theta-2\theta$ scan mode at variable rate depending on the reflection intensity was applied. The intensities were corrected for Lorentz and polarization effects and for absorption. The unit-cell dimensions were measured as a function of temperature by least-squares fits to 30−35 automatically centered reflections at fixed temperatures. The crystals were cooled/heated with a nitrogen stream using an Oxford Cryosystem device; the temperature was stabilized within 0.1 K.

The crystal structures were solved using the Patterson method with the SHELXS97 program[13] and refined by the full-matrix least-squares method on all F^2 data using the SHELXL97 program.[14] All of the heavy atoms were refined with anisotropic temperature factors. The H atoms were located from the molecular geometry, and their isotropic temperature factors U_{iso} were assumed to be 1.2 times the U_{eq} of their closest heavy atoms. The crystal data and experimental and refinement details are given in Table 1. The final atomic coordinates and equivalent temperature factors are listed in Table 2.

Results

Crystal Structures Description. At room temperature, $PyAuBr_4$ crystallizes in monoclinic space group *C*2/*m*. The crystal is built of sheets of pyridinium cations and squared tetrabromoaurate anions alternately stack along the [001] direction, as illustrated in Figure 1. Thus, the structure is the same as that of $PyAuCl_4$.[12] Because of the presence of strong X-ray scatterers in the structure and the cation disordering at room temperature,[9] the position of the nitrogen atom in the pyridinium ring could not be determined from the difference Fourier map. The $C_5NH_6^+$ ions occupy special positions of the site symmetry of 2/*m*, which imposes cationic disorder. Therefore, in the final stage of the structure refinement, the sites of the ring pyridinium atoms situated in the crystal mirror plane were assumed to be occupied by the N and C atoms at 50% probability, which satisfies the site symmetry of the cation. A similar model was previously proposed for isostructural $PyAuCl_4$.[12] But it should be stressed that the structure refinement with the ring atoms composed of 5/6C and 1/6N resulted in nearly the same R-factors, thus, it seems to be rather impossible to discriminate between the two models from the X-ray diffraction data. As seen in Figure 1, the planar ions are tilted from the average planes of the sheets, the pyridinium cations are inclined by 17.4(1.4)°, and the tetrabromoaurate anions are inclined by 7.61(9)° to the (001) plane. Such arrangements minimize electrostatic interactions between neighboring ions within the columns formed along [001].

Unlike that of the chloride and bromide compounds, the structure of $PyAuI_4$ does not have a layered character. The increase in the size of the anion (for comparison of the Au−Br and Au−I distances, see Table 3) results in a different crystal packing, as shown in Figure 2. The planes of the nearly squared AuI_4^- ions are inclined by about +45° or −45° to the (010) plane forming channels along [100]. The channels are occupied

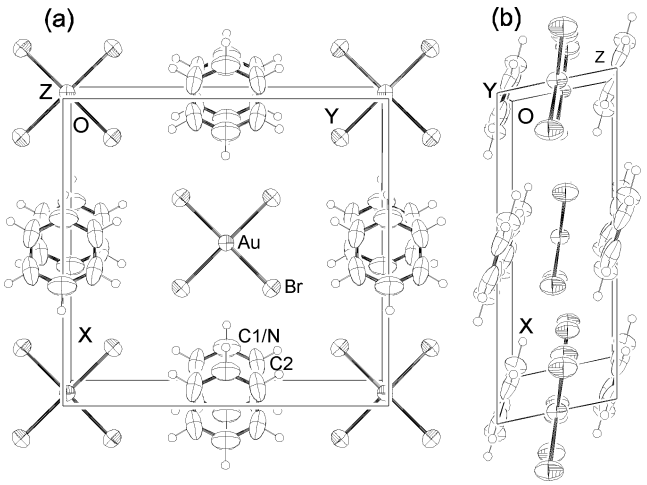

Figure 1. Crystal structure of $PyAuBr_4$ viewed (a) along [001] and (b) along [010]. The displacement ellipsoids are drawn at a 50% probability level, and the H atoms are represented as small circles.

TABLE 3: Selected Bond Lengths (Å) and Angles (deg) for $PyAuBr_4$ and $PyAuI_4$

	$PyAuBr_4$		
Au−Br	2.4126(15)	Br−Au−Br^b	89.70(7)
C(1)/N−C(2)	1.30(2)	Br−Au−Br	90.30(7)
C(2)−C(2^a)	1.44(4)	C(2)−C(1)/N−C(2^b)	126(2)
		C(1)/N−C(2)−C(2^a)	116.8(12)
	$PyAuI_4$		
Au−I(2)	2.617(2)	I(2)−Au−I(1^c)	90.12(7)
Au−I(1^c)	2.6190(16)	I(2) −Au−I(1^e)	89.88(7)
C(1)−C(2)	1.35(8)	C(3^c)−C(2)−C(1)	105(4)
C(2)−C(3^c)	1.24(6)	C(3^d)−C(1)−C(2)	125(4)
C(1)−C(3^d)	1.24(7)	C(2^f)−C(3)−C(1^g)	129(5)

Symmetry transformations used to generate equivalent atoms: ^a-x, y, $-z+2$; $^b x$, $-y+1$, z; $^c x$, $-y+3/2$, $z-1/2$; $^d-x+1$, $y+1/2$, $-z+1/2$; ^e-x, $y-1/2$, $-z+3/2$; $^f x$, $-y+3/2$, $z+1/2$; $^g-x+1$, $y+1/2$, $-z1/2$.

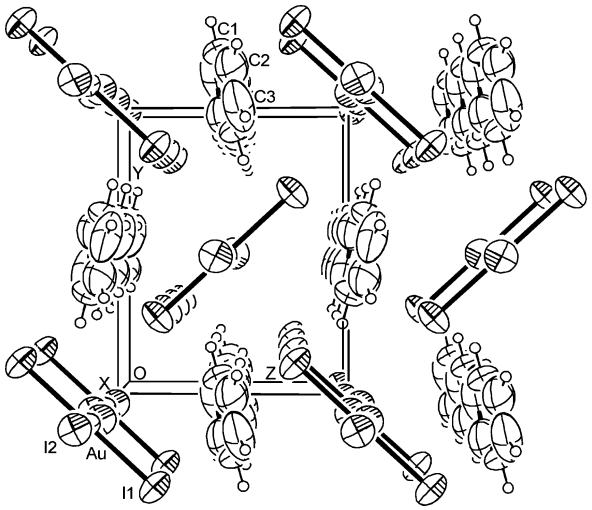

Figure 2. Crystal structure of $PyAuI_4$ viewed along [100]. The displacement ellipsoids are shown at a 50% probability level; the small circles represent the H atoms.

by the pyridinium cations. It is highly probable that, at room temperature, the cations are disordered around their pseudohexad axes, similar to what is observed in other simple pyridinium salts. The carbon and nitrogen atoms were indistinguishable in the refinement process of the structural model. Therefore, all of the pyridinium ring atoms were refined, for simplicity, as carbon atoms.

Thermal Expansion. Apparently, for $PyAuCl_4$ and $PyAuBr_4$, the deflections of the ions with respect to the (001) plane lead to a tighter packing along [100] when compared to that along [010]. Consequently, a considerable difference between the lattice translations a and b is observed (see Table 1 and Figure 3a). The temperature dependencies of the unit-cell parameters of both crystals are shown in Figure 3. The clear similarities in the thermal expansion of the crystal lattices of the chloride and bromide reflect their isostructural character. This is the reason for their similar anomalous temperature behavior. Although the parameters a and c decreasing with decreasing temperature is a normal effect, the expansion of the crystals along [010] is untypical. The parameters b elongate with decreasing temperature, reaching maximum values at ~180 K, and then contract slightly as the temperature is lowered further. The change in the sign of the linear expansion coefficient indicates that temperature changes essentially affect the ion−ion interactions along [010]. Such an effect is not observed for $PyAuI_4$, which exhibits a normal temperature behavior for the lattice parameters, as illustrated in Figure 4. Thus, it seems that the arrangement

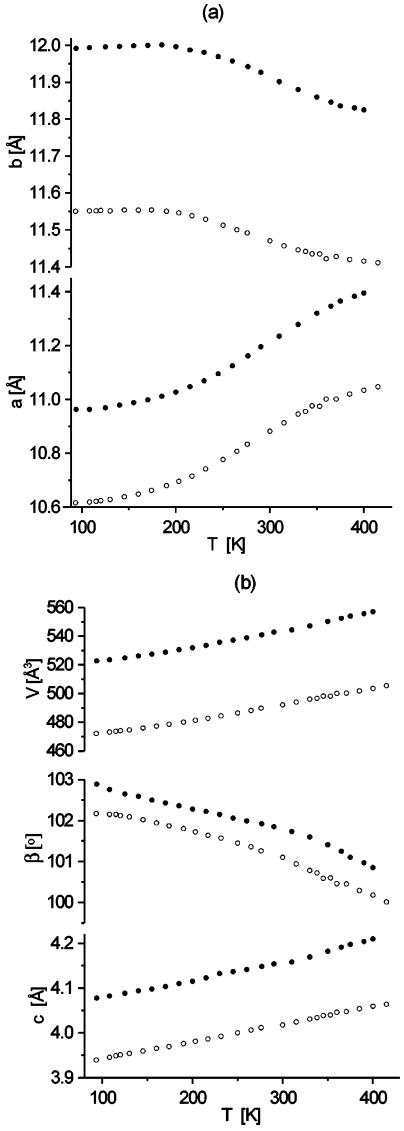

Figure 3. Temperature dependence of the unit-cell parameters a and b (a) as well as that of c, the monoclinic angle β, and the unit-cell volume V (b) for $PyAuCl_4$ (○) and $PyAuBr_4$ (●).

of the ions into sheets play a prominent role in determining the properties of the $PyAuCl_4$ and $PyAuBr_4$ crystals.

Dielectric Properties. The complex electric permittivity $\epsilon = \epsilon' - i\epsilon''$ was measured exclusively for polycrystalline $PyAuBr_4$. The results presented here are in general agreement with the previous study,[11] but we propose a new interpretation of the data. The temperature dependencies of the real and imaginary parts of the electric permittivity are plotted in Figure 5. Both dielectric functions show a profound dispersion in the low-temperature range below ~200 K. The maxima of ϵ' are shifted toward lower temperatures with decreasing frequency of the measuring electric field; additionally, the $\epsilon'(T)$ dependencies exhibit a cusplike shape, which is a characteristic feature of dipolar glasses. The high-temperature slopes of the $\epsilon'(T)$ dependencies obey the Curie−Weiss law: $\epsilon' - \epsilon_\infty = C/(T - T_0)$, in which ϵ_∞ is the high-frequency limit of electric permittivity, C is the Curie−Weiss constant, and T_0 is the Curie−Weiss temperature. The best fitting of the 30 kHz data, represented by the solid line in Figure 6, was obtained with the following parameters: $\epsilon_\infty = 4.5$, $C = 2721$ K, and $T_0 = -107.9$ K. The temperature T_f, marked by an arrow in Figure 6, indicates the point below which the Curie−Weiss law is violated. This

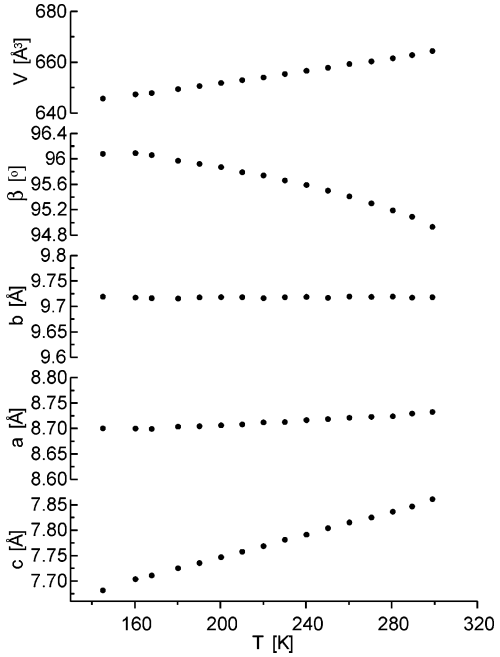

Figure 4. Temperature dependence of the lattice parameters of $PyAuI_4$.

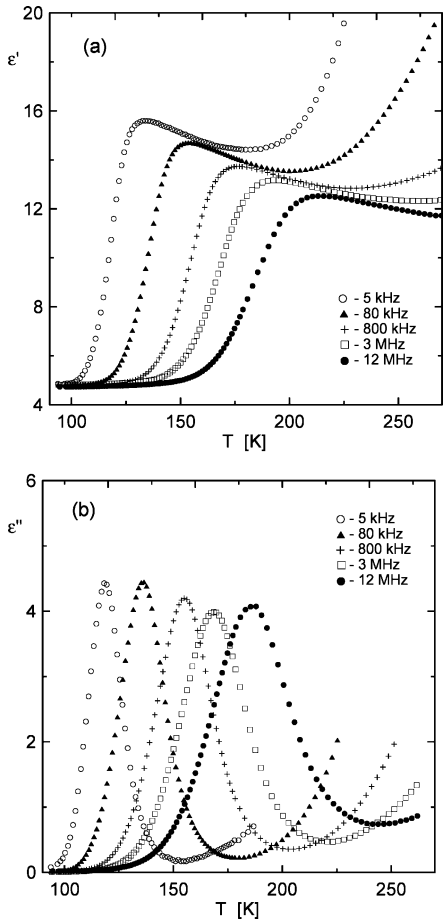

Figure 5. Temperature dependence of the real (a) and imaginary (b) parts of the complex electric permittivity measured for polycrystalline $PyAuBr_4$ at different frequencies.

temperature is frequency-dependent, and its presence indicates the onset of the formation of a dipolar glass state.

Analysis of the dielectric absorption as a function of frequency has shown that the absorption peak is somewhat broader (fwhm = 1.5 decades) than the 1.14 decades expected

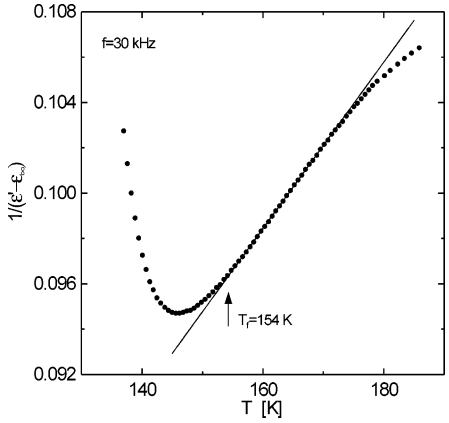

Figure 6. The Curie−Weiss fit of the 30 kHz electric permittivity of $PyAuBr_4$.

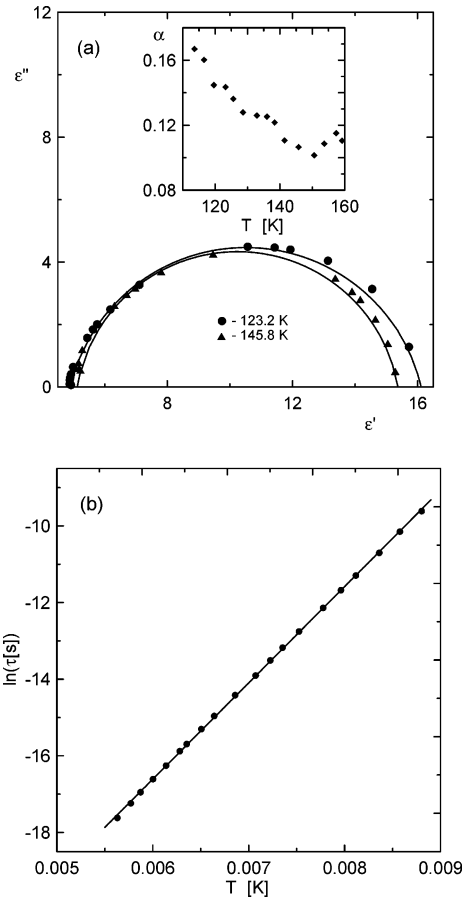

Figure 7. (a) Two exemplary Cole−Cole plots for $PyAuBr_4$ at 123.2 and 145.8 K; the solid lines represent the best fits of eq 1 to the experimental points. (b) Arrhenius plot, ln τ versus reciprocal temperature, for the most probable relaxation time; the solid line corresponds to the best fit of the Arrhenius equation. The inset in panel (a) shows the temperature dependence of the fit parameter α.

for a pure monodispersive Debye process, but the effect of the broadening is definitely not as profound as that reported for dipolar glassy behavior in mixed systems.[3] As shown in Figure 7a, the Cole−Cole plots form semiarcs with the centers located below the ϵ' axis, which also indicates a polydispersive character of the relaxation. In such a case, the complex electric permittivity can be described using the Cole−Cole function:[15]

$$\epsilon = \epsilon_\infty + \frac{\epsilon_s - \epsilon_\infty}{1 + (i\tau\omega)^{1-\alpha}} \qquad (1)$$

in which ϵ_s is a low-frequency value of the real part of electric permittivity, τ is the most probable relaxation time, α is a measure of the distribution of relaxation times, and $\omega = 2\pi\nu$ is the angular frequency. In Figure 7a, the fits of eq 1 to the experimental data at two different temperatures are represented by solid lines. The inset in this figure illustrates the temperature dependence of the exponent α. In the temperature range below 150 K, α increases with decreasing temperature, indicating a broadening in the distribution of the relaxation rates. However, it should be stressed that the magnitude of α is relatively small, and therefore one can anticipate that the spectrum of the relaxation times in $PyAuBr_4$ is significantly narrower when compared to that for the substances regarded as typical dipolar glasses, such as RADP[16] or $(BP)_x(BPI)_{1-x}$.[4,17] This property may be a consequence of the structural homogeneity of the single-component system for which the structural contribution to the distribution of the energy barriers and relaxation rates is essentially reduced.

The most probable relaxation time τ, derived from the fitting procedure of the Cole−Cole equation to the experimental data, is plotted as a function of temperature in Figure 7b. The $\tau(T)$ temperature dependence follows the Arrhenius law:

$$\tau = \tau_0 \exp\left(\frac{E_a}{k_B T}\right) \qquad (2)$$

in which E_a is the activation energy, and the preexponential, τ_0, is a reciprocal of the attempt jump frequency. An excellent fit to the experimental data ($R^2 = 0.9998$) was obtained with $E_a = 20.9$ kJ/mol and $\tau_0 = 1.73 \times 10^{-14}$ s. The activation energy is significantly higher than the 18 kJ/mol obtained earlier at the assumption of a single Debye-type relaxation process.[11] The parameters calculated from the fit can also be compared with the activation energies $E_A = 22.2$, $E_B = 17.4$, and $E_C = 13.7$ kJ/mol, and $\tau_0 = 7.0 \times 10^{-14}$ s, which is derived from a modeling of the ^{1}H NMR measurements for $PyAuBr_4$.[9] The authors interpreted their results by assuming three inequivalent energy barriers to the reorientation of the pyridinium cation around its pseudohexagonal symmetry axis, although they did not exclude an additional contribution from a continuous distribution of the energy barriers.

Discussion

A common unquestionable conclusion, arising both from the NMR and dielectric studies of $PyAuCl_4$ and $PyAuBr_4$, is the dynamical disordering of the pyridinium cation in the range of higher temperatures. Because of the in-plane 60° jumps, the electric dipole moment of the pyridinium ring assumes random orientations, which leads to a vanishing of its average value. The orientational freedom of the dipoles gives rise to a relatively high electric permittivity of the crystals. When the temperature is lowered, the in-plane reorientational motions slow, but the long-range ferroelectric or antiferroelectric arrangements of the dipoles are clearly not formed. Such processes must be associated with the phase transitions, seen as profound changes in the dielectric functions. Therefore, in our opinion, the transition observed in $PyAuBr_4$ at 99.9 K[11] cannot be interpreted in terms of the orientational ordering of the pyridinium ions. A closer inspection of the dielectric functions in the temperature range 80−120 K did not reveal any trace of dielectric anomaly (see Figure 8), which could be ascribed to the order−disorder transition in the dipolar sublattice of the crystal. Thus, the most probable scenario is that, in low temperatures, the pyridinium cations remain in random orientations with the long relaxation

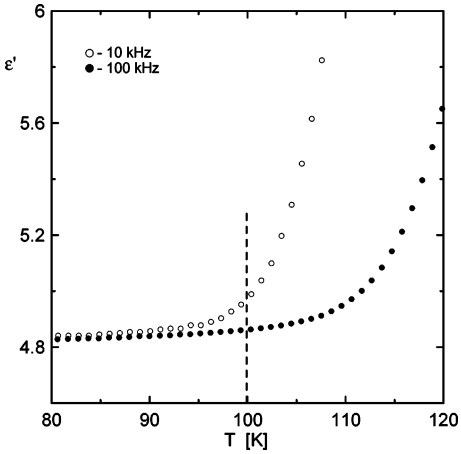

Figure 8. Temperature dependence of the dielectric constant of $PyAuBr_4$ at 10 and 100 kHz, measured in the vicinity of the phase transition reported in ref 11. The vertical dashed line marks the transition temperature.

times, forming a dipolar glassy state. This picture is consistent with the dielectric response of $PyAuBr_4$ and can also be reconciled with the anomalous thermal expansion of the $PyAuCl_4$ and $PyAuBr_4$ crystals. The layered arrangement of the ionic sheets results in a strong anisotropy of the crystal lattice. For example, in the $PyAuBr_4$ structure, the closest distance between the dipoles within the cationic column along [001] is 4.16 Å, whereas within the sheet it is 8.19 Å. A similar relation is observed in $PyAuCl_4$. Therefore, the dipole−dipole interactions within the sheets and along [001] must be different. This conclusion refers to the energy of the interactions and probably also to their character. The latter suggestion can be inferred from the strong anisotropy of the thermal expansion of both crystals. The large shortening of *a* and the simultaneous elongation of *b* with decreasing temperature can be explained by the nucleation and growth of a short-range ferroelectric-type order within the cationic sheets. The arrangement of neighboring cations in the form of clusters with the dipole moments parallel to the mirror symmetry-plane would result in an additional repulsive force between the rings along [010], and, simultaneously, an attractive contribution should occur along [100]. The slowing down of the pyridinium cation reorientations with decreasing temperature results in an enhancement of the clustering effect and, hence, the elongation of the crystal along [010]. At sufficiently low temperatures (below 200 K) the effect of the aggregation of the dipoles saturates, leading to the normal temperature dependence of the unit-cell dimensions of the crystal in low temperatures. The slowing of the dipolar entities also modifies the interplay between the sheets, which can be a reason for the phase transition at 99.9 K. Thus, the transition mechanism would be of displacive rather than order−disorder type, which is consistent with the lack of dielectric anomaly. On the other hand, at high temperatures the reorientations intensify, acting against the coupling of the dipoles. The progressive loss of correlations between the dipoles is seen as a nonlinear behavior of the temperature dependence of the lattice parameters *a* and *b* observed above 350 K (see Figure 3a). Thus, from the plots in Figure 3, the temperature range in which the short-range order of the dipoles plays a prominent role in the thermal expansion of the crystal can be roughly estimated to be from 180 to 400 K. Interestingly, this wide temperature range coincides with an unusually wide range of narrowing of the ^{1}H NMR line observed in $PyAuCl_4$ and $PyAuBr_4$,[9] which indicates the same molecular mechanism for these two phenomena.

The short-range ferroelectric interaction within the sheets is too weak to permeate the whole sheet and produce its macroscopic ferroelectric order, even at low temperatures. This is an important factor because, in such a case, the dipoles in different clusters are characterized by different orientations. Simultaneously, the close contacts between the dipoles along [001] favor their antiparallel couplings. Therefore, a competition between the short-range ferroelectric and antiferroelectric orders can occur in the dipolar sublattice of the crystal, leading to frustration effects and the development of a glassy state at low temperatures. Such effects are not expected in $PyAuI_4$, the structure of which is not layered.

Conclusions

The results of this study provided compelling evidence of the dipolar glass phase formation in the $PyAuBr_4$ and $PyAuCl_4$ crystals. These compounds are different from the materials commonly accepted as typical dipolar glasses because they are pure (undoped, nonirradiated) substances in which the disorder in the cationic sublattice is not artificially introduced but is rather their intrinsic feature. Because of this property, these crystals offer an opportunity for studying the development of a dipolar glass phase in compositionally homogeneous systems, similarly to what has been observed in $TlNO_2$ and CuCN pure crystals.[7,8] The relatively narrow distribution of the relaxation rates, inferred from the dielectric examinations of $PyAuBr_4$, can be one of the implications of the lack of the composition-induced lattice strains and deformations, although this problem requires further studies, especially in the low-frequency range. Another interesting thing is the source of frustration of the dipole−dipole interactions in these pure systems. It is plausible that the phenomenon arises from the specific properties of the crystal structure. The strong anisotropy of the crystal lattice results in a spatial differentiation of the dipolar interactions, and thus it is the reason for the occurrence of glassy state. Finally, it is worth noting that the onset of dipole−dipole correlations in $PyAuBr_4$ and $PyAuCl_4$ occurs at unusually high temperatures (∼400 K), about 300 K above the low-frequency electric permittivity maxima (∼100−120 K). This effect resembles the formation of polar nanoregions in ferroelectric relaxors at the Burns temperature.[18]

References and Notes

(1) Courtens, E.; Rosenbaum, T. F.; Nagler, S. E.; Horn, P. M. *Phys. Rev. B* **1984**, *29*, 515.
(2) Binder, K.; Young, A. P. *Rev. Mod. Phys*. **1986**, *58*, 801.
(3) Loidl, A.; Böhmer, R. In *Disorder Effects on Relaxational Processes*; Richert, R., Blumen, A., Eds.; Springer-Verlag: Berlin, Heidelberg, 1994; pp 659−696.
(4) Hutton, S. L.; Fehst, I.; Böhmer, R.; Braune, M.; Mertz, B.; Lunkenheimer, P.; Loidl, A. *Phys. Rev. Lett*. **1991**, *66*, 1990.
(5) Hanaya, M.; Nomoto, M.; Miura, T.; Oguni, M. *Solid State Commun*. **2000**, *115*, 57.
(6) Orešič, M.; Pirc, R. *Phys. Rev. B* **1993**, *47*, 2655.
(7) Johari, G. P.; Collins, M. F.; Feyerherm, R. *Phys. Rev. B* **2000**, *61*, 5827.
(8) Wang, J.; Johari, G. P. *Phys. Rev. B* **2003**, *68*, 214201.
(9) Ito, Y.; Asaji, T.; Ikeda, R.: Nakamura, D. *Ber. Bunsen-Ges. Phys. Chem*. **1988**, *92*, 885.
(10) Ishikawa, A.; Ito, Y.; Horiuchi, K.; Asaji, T.; Nakamura, D. *J. Mol. Struct*. **1989**, *19*, 2221.
(11) Fujimori, H.; Asaji, T.; Hanaya, M.; Oguni, M. *J. Therm. Anal. Calorim*. **2002**, *69*, 985.
(12) Adams, H.-N.; Strähle, J. *Z. Anorg. Allg. Chem*. **1982**, *485*, 65.
(13) Sheldrick, G. M. *SHELXS97: Program for Solution of Crystal Structures*; University of Göttingen: Göttingen, Germany, 1997.
(14) Sheldrick, G. M. *SHELXL97: Program for Crystal Structure Refinement*; University of Göttingen: Göttingen, Germany, 1997.
(15) Cole, K. S.; Cole, R. H. *J. Chem. Phys*. **1941**, *9*, 341.
(16) Courtens, E. *Phys. Rev. Lett*. **1984**, *52*, 69.
(17) Banys, J.; Klimm, C.; Völkel, G.; Bauch, H.; Klöpperpieper, A. *Phys. Rev. B* **1994**, *50*, 16751.
(18) Burns, G.; Dacol, F. H. *Phys. Rev. B* **1983**, *28*, 2527.